Molecular Dynamics Computation of Steady-State Sputter Yields of Hexagonal Boron Nitride

IEPC-2015-278／ISTS-2015-b-278

Presented at Joint Conference of 30th International Symposium on Space Technology and Science, 34th International Electric Propulsion Conference and 6th Nano-satellite Symposium
Hyogo-Kobe, Japan
July 4–10, 2015

Brandon D. Smith* and Iain D. Boyd†
University of Michigan, Ann Arbor, Michigan, 48109, USA

Abstract: The sputtering of *h*-BN by energetic xenon ions is investigated using a high-fidelity, high-speed molecular dynamics (MD) model. Both integrated and differential sputter yields are computed over a range of ion energies from 20 eV to 300 eV, and incidence angles from 0° to 75°. Sputtering is shown to occur at energies as low as 40 eV, suggesting a threshold energy between 30 eV and 40 eV. The integrated yields at 0° incidence are compared to existing experimental data and are shown to agree well over the range of ion energies investigated. Bohdansky curve fits are performed in order to calculate the threshold energy, giving results of 36 ± 3 eV and 48 ± 9 eV depending on the initial parameters used. These results are shown to compare well with experimental observations that the threshold energy lies between 30 and 40 eV. The calculated differential yields are compared to experimental measurements, showing excellent qualitative agreement. The velocity distribution of sputtered boron atoms is also investigated. The Sigmund-Thompson distribution function predicted by linear cascade theory is fit to the simulation data and is shown to match the data very well. The average surface binding energy computed from the Sigmund-Thompson fits is found to be 4.5 eV for ion energies of 100 eV and greater. This compares well to the experimentally observed binding energy of 4.8 eV.

Nomenclature

E	= kinetic energy of the incident ion
E_b	= surface binding energy
E_{th}	= threshold energy for sputtering
E^*	= characteristic energy in the modified Zhang function
N	= number of ion impacts
N_B, N_N	= number of boron and nitrogen atoms ejected
T	= system temperature
T_0	= desired equilibrium temperature
Y_{total}	= integrated sputter yield computed from sum of boron and nitrogen atoms ejected
Y_{est}	= integrated sputter yield extrapolated from boron atoms ejected
Z_i	= atomic number of atom i
a_0	= Bohr radius
f_{ST}	= Sigmund-Thompson velocity distribution function
m_B, m_N	= molecular mass of boron and nitrogen

*Ph.D. candidate, Department of Aerospace Engineering, bradenis@umich.edu
†James E. Knott Professor, Department of Aerospace Engineering, iainboyd@umich.edu

m_{ST}	= fit parameter in the Sigmund-Thompson VDF
r_{ij}	= distance between atoms i and j
v	= particle velocity
v_b	= effective binding velocity in the Sigmund-Thompson VDF
y	= differential sputter yield
Φ_{AM}, Φ_{ZBL}	= Albe-Möller and Ziegler-Biersack-Littmark potential functions
ρ_{BN}	= mass density of h-BN
τ	= time constant for Berendsen thermostat
θ_{ijk}	= bond angle between atoms i, j, and k
θ_{ion}	= ion incidence angle relative to surface normal
θ	= polar angle at which a particle is ejected
ϕ	= azimuthal angle at which a particle is ejected

I. Introduction

Historically, the life-limiting mechanism of Hall thrusters has been the erosion of the discharge channel walls via ion bombardment. These walls, usually made of hexagonal boron nitride (h-BN) or some BN-based ceramic, shield the magnetic coils and pole pieces from the plasma discharge. During thruster operation, energetic ions from the plasma strike the walls, resulting in atomic sputtering. Over time, these sputtering events accumulate to produce macroscopic erosion of the walls, ultimately exposing the magnetic circuit to the plasma. The subsequent erosion of the pole pieces changes the magnetic topography in the thruster and eventually leads to thruster failure. The erosion process also produces free condensible material, which may redeposit elsewhere in the thruster, possibly reducing the effective erosion rate, or on spacecraft surfaces, possibly interfering with solar panels or optical instruments. Hence, characterizing the erosion of h-BN is of critical importance both in thruster lifetime estimation and in revealing possible spacecraft integration issues.

The operational lifespan of Hall thrusters has traditionally been determined by operating the thruster under high-vacuum conditions until failure. Such tests are both time-consuming and very expensive, requiring thousands of hours of total operation for both the thruster and the vacuum facilities. In order to mitigate costs and accelerate the process of lifetime validation, there has been considerable effort towards understanding the atomic sputtering process that underlies wall erosion. For a given material, the number of atoms ejected per incident particle—called the integrated sputter yield—is a function of the kinetic energy of the incident particle and its angle of incidence with respect to the material surface. There have been several attempts at determining the sputter yields of h-BN experimentally through measurement techniques such as mass loss,[1–4] cavity ring-down spectroscopy (CRDS),[4] and quartz crystal microbalance (QCM).[5] However, these efforts have provided very limited data in the energy range of greatest interest in Hall thrusters (tens to hundreds of eV) because the sputter yields fall below the measurement threshold of the devices used. Thus, the utility of these measurements in estimating Hall thruster erosion and lifetime was limited. Furthermore, none but the QCM measurements provided information on the spatial distribution of sputtered particles—the differential sputter yields—that could be used to describe the behavior of ejected particles as they move into the ambient environment.

High-fidelity, physics-based modeling offers a unique means of filling the gaps in the experimental data. This motivated Yim and Boyd to develop a molecular dynamics (MD) model[6] to simulate the sputtering of pure h-BN under xenon ion bombardment. This model demonstrated the feasibility of MD for computing integrated sputter yields of h-BN, but could not produce sufficient statistics for computing differential sputter yields. Smith and Boyd continued developing the model,[7] demonstrating the preferential sputtering of nitrogen during the initial stages of ion bombardment, and thus the need for extended simulations to achieve steady-state conditions. In this work, we present the most recent results of the sputtering model: steady-state integrated and differential sputter yields of h-BN as a function of the kinetic energy and incidence angle of the impacting ions, with an emphasis on ion energies of 100 eV or less.

The remainder of this paper is organized as follows: Section II discusses the details of the numerical model used. Section III presents the simulation results, including integrated and differential sputter yields and the velocity distribution functions of sputtered boron, and compares the results to experimental measurements. Finally, Section IV summarizes our findings and outlines possibilities for future work.

II. Model overview

A. Molecular dynamics framework

The sputtering model used in this work is an application of the molecular dynamics (MD) method. In MD, atoms are treated as classical particles that interact through analytical interatomic potential functions. At each time step, the net force acting on each atom is computed as the sum of forces exerted by all nearby atoms. Then, the position and velocity of each atom are integrated in time according to Newtonian mechanics to reach a new system state. This cycle repeats until the desired macroscopic properties are determined with sufficient statistical certainty.

The MD framework used for the sputtering model is HOOMD-blue.*,[8] HOOMD-blue is an open-source, general purpose MD code that utilizes Nvidia's CUDA computing architecture[9] to utilize the massively

*HOOMD-blue web page: `http://codeblue.umich.edu/hoomd-blue`

parallel processing capabilities of graphics processing units (GPUs). GPUs excel at performing floating-point arithmetic on large sets of data, such as the calculations involved in MD. This allows for a reduction of two or more orders of magnitude in wall time compared to a single CPU core. For sputtering simulations, this allows many more ion impacts to be processed in a given amount of time, improving the statistical confidence of the resulting sputter yields. GPUs are also inexpensive compared to CPU-based computing clusters of similar performance, costing only a few hundred to a few thousand US dollars. This combination of large performance benefits and relatively low cost make HOOMD-blue an ideal tool for this work.

B. Interatomic potentials

The sputtering model utilizes two separate interatomic potential functions: one to define the interactions between the boron and nitrogen atoms in the BN lattice, and another to define the interactions between the impacting xenon ion and the lattice atoms. The intra-lattice interactions are defined by a Tersoff-like many-body potential developed by Albe et al. specifically for boron nitrides:[10,11]

$$\Phi_{AM} = \frac{1}{2}\sum_{i\neq j} f_C\left(r_{ij}\right)\left[f_R\left(r_{ij}\right) + b_{ij} f_A\left(r_{ij}\right)\right]. \tag{1}$$

The repulsive and attractive terms take the form of a Morse potential:

$$\begin{aligned} f_R\left(r_{ij}\right) &= \frac{D_0}{S-1}\exp\left(\beta\sqrt{2S}\left(r-r_0\right)\right), \\ f_A\left(r_{ij}\right) &= \frac{SD_0}{S-1}\exp\left(\beta\sqrt{2/S}\left(r-r_0\right)\right). \end{aligned} \tag{2}$$

The coefficient b_{ij} modifies the attractive term of the potential to account for factors such as the total number of bonded parters and the bond angles. It takes the form

$$\begin{aligned} b_{ij} &= \left(1+\gamma^n\chi_{ij}^n\right)^{-1/2n}, \\ \chi_{ij} &= \sum_{k\neq i,j} f_C\left(r_{ik}\right) g\left(\theta_{ijk}\right)\exp\left(\lambda^3\left(r_{ij}-r_{ik}\right)^3\right), \\ g\left(\theta_{ijk}\right) &= 1+\frac{c^2}{d^2}-\frac{c^2}{d^2+\left(h-\cos\theta_{ijk}\right)^2}. \end{aligned} \tag{3}$$

Finally, f_C is a cutoff function that limits the interaction range between atoms in order to reduce the computational cost of the simulation. It forces the potential to transition smoothly to zero at some finite distance as follows:

$$\begin{aligned} f_C\left(r\right) &= \begin{cases} 1, & r \leq R-D \\ \exp\left(\dfrac{3\hat{r}^3}{\hat{r}^3-1}\right), & R-D < r < R+D \\ 0, & r \geq R+D \end{cases}, \\ \hat{r} &= \frac{r-(R-D)}{2D}. \end{aligned} \tag{4}$$

In Eqs. 2–4 the variables D_0, S, r_0, β, γ, n, λ, c, d, h,R, and D are parameters specific to each ij species pairing: B–B, B–N, and N–N. The parameters for each pair are given in Table 2. Note that the parameters c and d for B–B interactions differ from those found by Albe et al. Yim found in his work[6] that the original values of c and d resulted in very high sensitivity to the bond angle about the equilibrium angle determined by h, thus mandating a very small time step to resolve the atomic motion. Yim instead adjusted the values of c and d while maintaining the same ratio c^2/d^2, making the simulations more tractable. We have chosen to keep Yim's values in spite of the performance gains afforded by HOOMD-blue because of the large number of ion impacts required to reach steady-state sputtering conditions.

Table 2: Pair specific parameter values for the Albe-Möller potential.

	B–B	B–N	N–N
D_0, eV	3.08	6.36	9.91
r_0, Å	1.59	1.33	1.11
S	1.0769	1.0769	1.0769
β, Å^{-1}	1.5244506	2.043057	1.92787
γ	1.6×10^{-6}	1.1134×10^{-5}	1.9251×10^{-2}
n	3.9929061	0.364153367	0.6184432
λ, Å^{-1}	0	1.9925	0
c	3.316257	1092.9287	17.7959
d	0.01	12.38	5.9484
h	0.5	-0.5413	0
R, Å	2.0	2.0	2.0
D, Å	0.1	0.1	0.1

The interactions between the impacting xenon ion and the boron and nitrogen atoms in the lattice are modeling using the Ziegler-Biersack-Littmark (ZBL) potential. It is a screened Coulomb potential of the form

$$\begin{aligned} \Phi_{ZBL}\left(r_{ij}\right) &= \frac{Z_i Z_j e^2}{4\pi\varepsilon_0 r_{ij}} \phi_{ZBL}\left(\frac{r_{ij}}{a_F}\right), \\ \phi_{ZBL}\left(x\right) &= \sum_{k=1}^{4} A_k \exp\left(B_k x\right), \\ a_F &= \frac{0.8853 a_0}{Z_i^{0.23} + Z_j^{0.23}}, \end{aligned} \tag{5}$$

where A_k and B_k are dimensionless parameters given in Table 3. One should note that while the impacting particle is referred to as the "ion" in this work, its charge state is not explicitly included in the MD model. Instead, the ZBL potential is assumed to be valid regardless of the impacting particle's charge state. In a real system, it is likely that a xenon ion impacting a BN surface will reflect as a neutral by absorbing an electron from the surface. However, the label of "ion" will be used for the remainder of this work for convenience.

Table 3: ZBL potential parameters.

k	1	2	3	4
A_k	0.1818	0.5099	0.2803	0.02817
B_k	3.2	0.9423	0.4029	0.2016

C. Domain configuration and simulation progression

Figure 1 shows an example h-BN lattice for use in the MD simulations. The xy-plane defines the surface plane of the h-BN and the z-axis defines the surface normal. This lattice represents a very small section at the exposed surface of a semi-infinite slab of BN. Hence, the boundary conditions in x and y are periodic, whereas those in z are open, allowing particles to leave the domain. The size of the lattice is specified by the number of graphene-like sheets (x direction), the number of side-to-side hexagons (z direction), and the number of point-to-point hexagons (y direction). The size of each hexagon is specified by the lattice constants a and s, and the spacing between the sheets is determined by the lattice constant c. The values of the lattice parameters are given in Table 4. In order to prevent the lattice from drifting or rotating, the bottommost layer of atoms (i.e., those having the lowest z position) are fixed in

Table 4: Lattice constants for h-BN.[10]

Lattice constant	Length, Å
a	2.496
c	3.245
s	1.441

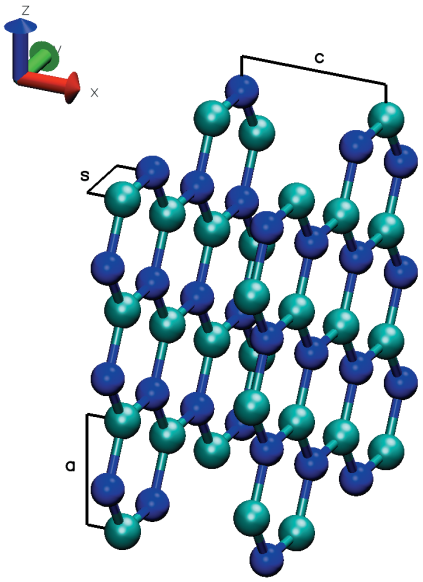

Figure 1: Sample domain for sputtering simulations with definitions for the lattice constants a, c, and s. Graphic generated using VMD software.[12]

space. These atoms are called the "immobile" atoms. The two layers of atoms above the immobile layer are dubbed the "thermostat" layers. They regulate the temperature of the lattice via a Berendsen thermostat,[13] which scales the velocity of the thermostat atoms by a factor based on the current system temperature:

$$\lambda_B = \sqrt{1 + \frac{\Delta t}{\tau}\left(\frac{T_0}{T} - 1\right)}. \tag{6}$$

In general, the size of the initial lattice for each simulation case depends on the ion energy and incidence angle being investigated. The domain size in the x and y directions must be just large enough that the energy cascade from the ion impact does not cross the periodic boundary conditions and resonate with itself. If these dimensions are too small then the calculated sputter yields may be artificially inflated due to this nonphysical resonance. Typically, the domain measures 24 sheets by 18 point-to-point hexagons for ion energies less than 100 eV, 32 sheets by 24 point-to-point hexagons for ion energies between 100 eV and 250 eV, and 12 sheets by 30 point-to-point hexagons for ion energies greater than 250 eV. Domain convergence studies are performed where feasible in order to ensure that the results are domain-independent.

Determining the domain size in the z direction is more complicated. Simply put, it must be large enough that the immobile and thermostat atoms have no immediate effect on the transfer of energy from the impacting ion to the atoms near the surface. Initially, this dimension is set to 10–14 side-to-side hexagons. After subsequent ion impacts, however, the z dimension of the lattice shrinks due to the loss of surface atoms. In a previous publication[7] it was demonstrated that when starting from a perfect h-BN lattice, nitrogen is sputtered preferentially over boron until a sufficiently deep layer of pure, amorphous boron is established at the surface. The thickness of this layer is limited by how deep the impacting ions can penetrate into the lattice. Thus, one can use the ratio of remaining nitrogen atoms to remaining boron atoms as a measure of how eroded the surface is. This ratio is evaluated before each ion is injected into the system. If the ratio is less than 0.4, then two additional side-to-side hexagons are added to the bottom of the lattice, increasing the depth of the lattice to compensate for surface erosion. The ratio is then reevaluated and the process is repeated until a ratio greater than 0.4 is established.

Once the initial lattice is generated, it is possible to begin simulating ion impacts and collecting data. As noted above, however, the early stages of sputtering consist of preferential removal of nitrogen from the surface layers and amorphization of the remaining boron. Under steady state conditions, boron and nitrogen must be sputtered at the 1:1 stoichiometric ratio of bulk BN, so it is desirable to shorten this initial

amorphization process. Thus, after the initial lattice is generated, a pre-processing script is used to randomly remove nitrogen atoms from a user-specified number of near-surface layers. The positions of the remaining boron atoms are then randomly perturbed, with each move being accepted only if the total potential energy of the system decreases. Once a set number of consecutive moves are rejected, 50 ion impacts are processed to remove any loosely bound atoms from the system before collecting sputter yield data.

Each ion impact is simulated by placing the xenon ion in the domain at the upper bound in the z direction with a prescribed kinetic energy and incidence angle. The incidence angle is defined as the angle between the ion velocity vector and the BN surface normal such that 0° corresponds to normal incidence. The position of the ion in x and y and the azimuthal angle of its velocity vector are randomized for each impact in order to minimize the influence of the lattice orientation on the resulting sputter yields. The initial velocities of the lattice atoms are sampled from a Maxwell-Boltzmann distribution at the desired equilibrium temperature. The position and velocity of each particle are integrated according to a second-order velocity-Verlet scheme with a time step of 0.1 fs. When a particle passes the upper z boundary, it is flagged as leaving the system. If the particle is an ion, its information is simply output to a text file for post-processing. If the particle is a nitrogen or boron atom, then any neighboring boron or nitrogen atoms are also flagged. The group of particles is treated as a molecule, and its information output to a text file for post-processing.

Each ion impact requires a minimum of 20,000 time steps to process. Each time a particle leaves the system an additional 10,000 time steps are allotted to allow enough time for any remaining sputtered or reflected particles to reach the z boundary. Further time steps are allotted to allow the lattice to relax to a thermal equilibrium defined by $T \in (0.9T_0, 1.1T_0)$. The equilibrium temperature T_0 is set to 150°C to match the sample temperature reported in sputtering experiments.[2,4] The system temperature is monitored using a sub-relaxation technique[14] in order to reduce the effect of instantaneous temperature fluctuations.

D. Data reduction

The raw outputs of the sputtering model are the time of ejection, species, kinetic energy, polar ejection angle, and azimuthal angle of each particle that passes the upper z boundary. The ejection angle is defined as the angle between the ejected particle's velocity vector and the surface normal such that an angle of 0° corresponds to a particle ejected normal to the surface. These data must be reduced in order to find the integrated and differential sputter yields. The integrated sputter yield is computed as the average number of boron and nitrogen atoms lost from the surface over some number of ion impacts N:

$$Y_{total} = \frac{N_B + N_N}{N} \tag{7}$$

where Y is measured in units of atoms/ion. To convert this to units of mm^3/C:

$$Y\left[\mathrm{mm}^3/\mathrm{C}\right] = Y\left[\text{atoms/ion}\right] \times \frac{0.5\left(m_B + m_N\right)}{e\rho_{BN}}.$$

As noted above, previous work with the MD sputtering model demonstrated that the sputter yield displays pronounced non-monotonic behavior when beginning from a perfect h-BN lattice. The behavior of the sputter yield correlates almost exactly with changes in the ejection rate of nitrogen, whereas the ejection rate of boron remains nearly constant. Thus, one can extrapolate the integrated sputter yield of both species combined from the yield of boron alone:

$$Y_{est} = \frac{2N_B}{N} \tag{8}$$

Under steady-state conditions, the yields calculated from Eqs. 7 and 8 are equal. However, Eq. 8 is a reliable calculation for the steady-state sputter yield even during the early stages of ion bombardment. Figure 2 shows the rate of ejection of boron as a function of ion fluence for a selection of MD cases ranging from 60 eV to 250 eV ion energy at normal and 60° incidence. Aside from statistical noise in the moving average, the rate of ejection of boron is nearly independent of ion fluence except over the first few thousand ion impacts, with lower-energy cases requiring more ion impacts for the boron ejection rate to stabilize. Thus, Y_{est} is considered an accurate calculation for the steady-state sputter yield.

Differential sputter yields are computed by generating a virtual hemisphere centered at the origin of the ejected particles, separating the hemisphere into slices of equal solid angle, and recording each particle that

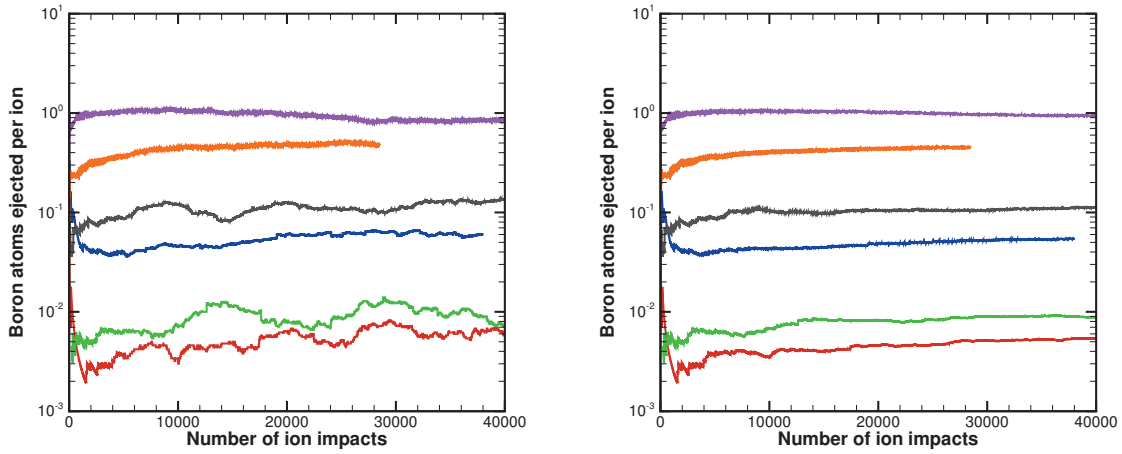

(a) **(b)**

Figure 2: Rate of ejection of boron for a selection of simulation cases. (a) shows a moving average with a period of 5000 ion impacts and (b) shows a cumulative average over all ion impacts.

passes through each section. The differential yield is then evaluated as

$$y\left(\theta,\phi\right)=\frac{N_B\left(\theta,\phi\right)+N_N\left(\theta,\phi\right)}{N} \tag{9}$$

where θ and ϕ define the centroid of each section of the hemisphere. To compare these data to experimental measurements, we can fit a modified Zhang function[15,16] in a least-squares sense:

$$\begin{aligned} y_{MZ}\left(\theta,\phi\right)=&\frac{Y}{1-\sqrt{\frac{E^*}{E}}\cos\left(\theta_{ion}\right)}\times\frac{\cos\left(\theta\right)}{\pi}\\ &\times\left[1-\frac{1}{4}\sqrt{\frac{E^*}{E}}\left(\cos\left(\theta_{ion}\right)\psi\left(\theta\right)+\frac{3\pi}{2}\sin\left(\theta_{ion}\right)\sin\left(\theta\right)\cos\left(\phi\right)\right)\right],\\ \psi\left(\theta\right)=&\frac{3\sin^2\left(\theta\right)-1}{\sin^2\left(\theta\right)}+\frac{\cos^2\left(\theta\right)\left(3\sin^2\left(\theta\right)+1\right)}{2\sin^3\left(\theta\right)}\times\ln\left(\frac{1+\sin\left(\theta\right)}{1-\sin\left(\theta\right)}\right). \end{aligned} \tag{10}$$

where E^* is a characteristic energy and $\phi=0$ corresponds to the forward sputtering direction. The ratio E^*/E is treated as a free fit parameter that controls the degree to which the sputtering is diffuse or cosine-like, with $E^*/E=0$ corresponding to purely diffuse sputtering.

The results of the MD model can also be used to compute the velocity distribution functions (VDFs) for the ejected particles. For a given species, the particle velocities are placed into discrete bins in velocity space. Analytical functions can then be fit to the resulting histograms. In particular, the volume-based Sigmund-Thompson[17,18] distribution is fit to the particle velocities along the surface normal direction:

$$f_{ST}\left(v\right)\propto\frac{v^2}{\left(v^2+v_b^2\right)^{3-2m_{ST}}}. \tag{11}$$

Note that, in the previous work,[7] the flux-biased Sigmund-Thompson distribution was used. However, the use of a flux-biased distribution was incorrect. Flux-biased distributions arise when tracking the VDF of particles passing through a plane from an infinite reservoir. Because faster-moving particles are more likely to pass the sampling plane within a given amount of time, the VDF appears to be biased by a factor of v. If the reservoir is finite and the sampling time is long enough to collect all particles from the reservoir,

then the bias disappears. In the sputtering simulations, each sputtering event behaves like a finite reservoir problem in which the sensor waits to capture all escaping particles. Thus, the volume-based VDF should be used in place of the flux-biased VDF.

III. Results and discussion

A. Total sputter yields

1. *Dependence on ion energy*

Figure 3 shows the integrated sputter yield of *h*-BN at normal ion incidence as a function of ion energy. The total yields are calculated according to Eq. 7, whereas the estimated yields are computed according to Eq. 8. The error bars on the estimated sputter yields are computed as $Y_{est}/\sqrt{N_B}$. Also shown in Fig. 3 are the QCM measurements of Rubin et al. for HBC grade boron nitride.[5] The data labeled QCM low correspond to the uncorrected QCM measurements and capture only condensible species. The data labeled QCM high are the QCM measurements corrected to include non-condensible species. This data set is chosen for comparison because it is the most comprehensive data set known to the authors, extending down to 60 eV incident ion energy and covering incidence angles from 0° to 45°.

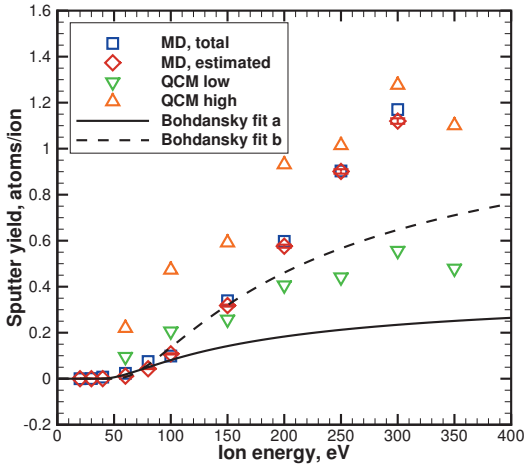

Figure 3: Sputter yield of *h*-BN at normal incidence as a function of incident ion energy.

Figure 3 indicates that the total and estimated sputter yields computed from the MD data agree very well, as would be expected under steady-state conditions. Both sets of sputter yields increase with increasing ion energy, as expected in the plotted range of energies. At ion energies of 100 eV and below, the calculated yields fall below the lower bound of the QCM measurements. For ion energies between 150 eV and 300 eV, the calculated yields fall within the bounds of the QCM measurements. However, extrapolating the yields past 300 eV suggests that the calculated yields will become greater than the QCM measurements. Overall, the calculated yields agree reasonably well with the measured values within the range of ion energies investigated here, suggesting that the MD model is largely capturing the appropriate physics.

The black curves in Fig. 3 are Bohdansky fits[19] to the estimated sputter yields:

$$Y_B = \alpha \left[1 - \left(\frac{E_{th}}{E}\right)^{2/3}\right]\left(1 - \frac{E_{th}}{E}\right)^2. \tag{12}$$

Rather than minimizing $\sum (Y_{fit} - Y)^2$, this equation is fit by minimizing

$$\sum \left(\frac{(Y_{fit} - Y)}{Y}\right)^2.$$

This fitting process limits the bias towards larger values, making it more appropriate for cases such as this in which data points can vary widely in magnitude. The fit parameters α and E_{th} are given random initial values during the least-squares fitting process, resulting in one of the two converged sets of parameters given in Table 5. The parameter α is the sputter yield in the limit of $E \to \infty$, whereas E_{th} is the threshold energy for sputtering. The threshold energy is of particular interest in Hall thrusters because most of the ions that contribute to wall erosion have kinetic energies near the threshold. The two curve fits here give values of 36 ± 3 eV and 48 ± 9 eV for the threshold energy. The lowest ion energy for which

Table 5: Bohdansky parameter values for normal ion incidence. The error is computed based on 95% confidence bounds from the least-squares fitting process.

	α, atoms/ion	E_{th}, eV
Fit a	0.4 ± 0.3	36 ± 3
Fit b	1.3 ± 1.1	48 ± 9

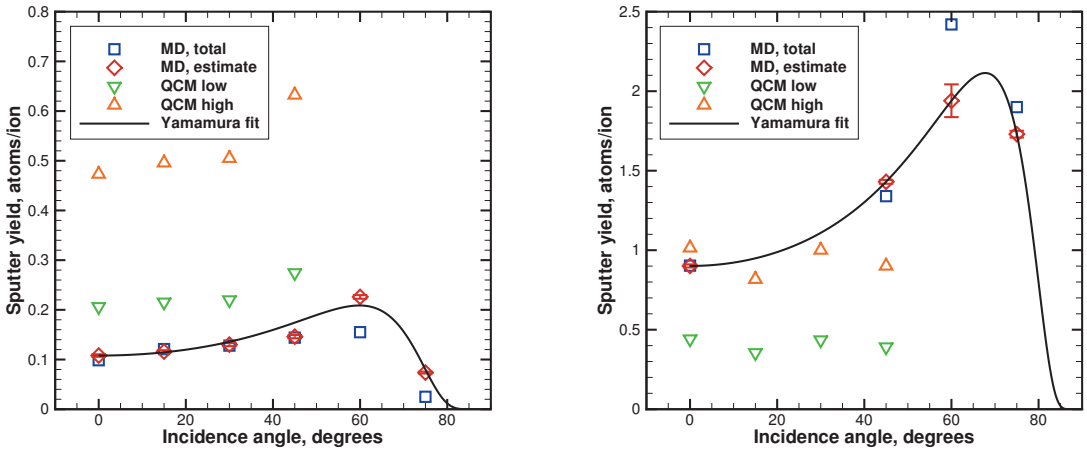

Figure 4: Total sputter yield as a function of ion incidence angle for (a) 100 eV and (b) 250 eV incident ion energy.

the MD model results in a finite sputter yield is 40 eV, suggesting a threshold energy between 30 and 40 eV. Similarly, a Bohdansky fit to the QCM data gives a threshold energy of 32 ± 6 eV, and Rubin claims that the QCM also detected BN sputtering at energies as low as 40 eV, although the data were not reported.[5] Thus, the MD model and Rubin's QCM measurements agree that the threshold energy for sputtering of *h*-BN sputtering most likely falls between 30 eV and 40 eV.

It is worth noting that the Bohdansky fits do not match the calculated sputter yields very well at energies above 100–150 eV. While this may be a result of the fitting process used, it may also be an indication that there is some bias in the results at those energies. One possibility is that these cases are not domain independent, causing the calculated sputter yields to be artificially inflated. Establishing domain independence for cases of high ion energy is especially difficult because increasing the domain size also increases the computational cost of the simulation. Since the near-threshold regime of sputtering is generally considered more important in Hall thrusters, this task is left for future work.

2. Dependence on incidence angle

Figure 4 shows the calculated *h*-BN sputter yields as a function of ion incidence angle for 100 eV and 250 eV incident ion energy. The estimated sputter yields are defined as in Eq. 8 above. Also plotted are Rubin's QCM measurements and a Yamamura fit to the estimated yields:[20,21]

$$Y_Y\left(\theta_{ion}\right) = Y\left(0^\circ\right)\cos^A\left(\theta_{ion}\right)\exp\left[-B\left(\frac{1}{\cos\left(\theta_{ion}\right)}-1\right)\right]\left[\frac{1-\sqrt{\frac{E_{th,Y}}{E}}\cos\left(\theta_{ion}\right)}{1-\sqrt{\frac{E_{th,Y}}{E}}}\right] \tag{13}$$

where A, B, and $E_{th,Y}$ are treated as best-fit parameters, although $E_{th,Y}$ is interpreted as the threshold energy for sputtering. The Yamamura curve is fit to the computed yields in the typical least-squares sense with random initial parameters. The calculated fit parameters are shown in Table 6 for several ion energies.

Figure 4 shows that at 100 eV, the computed sputter yields fall outside the bounds of the QCM data for all available angles of incidence. This is not surprising given that Fig. 3 showed that the computed sputter yields are comparatively low for energies less than about 100 eV. At 250 eV, all of the computed yields except that at normal incidence fall outside the range of the QCM measurements, but this is again consistent with the observations in Fig. 3. For both 100 eV and 250 eV, the Yamamura curve fits the computed sputter yields very well, showing a peak in the sputter yield between 60° and 70° incidence. However, Table 6 shows that the calculated value of $E_{th,Y}$ is approximately zero for all investigated ion energies for which a converged

Table 6: Yamamura fit parameters for several ion energies.

Ion energy	A	B	$E_{th,Y}$, eV
60 eV	-4.2	2.3	0.0
80 eV	-2.8	1.6	0.0
100 eV	-3.5	1.7	0.0
200 eV	-2.9	1.2	0.0
250 eV	-2.4	0.92	0.0

Table 7: $^{E^*}/_E$ from the modified Zhang fits to the calculated differential sputter yields and to the QCM measurements of HBC-grade BN from Ref. 5.

Ion energy, eV	Incidence angle	E^*/E	
		MD	QCM
100	0°	0.0	0.18
	15°	0.0	0.13
	30°	0.01	0.18
	45°	0.13	0.21
	60°	0.27	—
	75°	0.74	—
250	0°	0.0	0.25
	45°	0.15	0.34
	60°	0.61	—
	75°	1.2	—

curve fit was found. All of these ion energies except for 60 eV are well above the threshold energy E_{th} computed from the Bohdansky fit, so it is not clear whether the low values of $E_{th,Y}$ are cause for concern. While $E_{th,Y}$ is commonly interpreted as the threshold energy for sputtering, its physical significance is not immediately apparent in the shape of the curve. For the purposes of this work, $E_{th,Y}$ will be interpreted as a best-fit parameter without any physical significance, whereas E_{th} will be interpreted as the threshold energy for sputtering.

B. Differential sputter yields

Figures 5 and 6 show the calculated differential sputter yields at 100 eV incident ion energy and the modified Zhang fits to those yields, respectively. Figures 7 and 8 show similar results for 250 eV ion energy. Note that these contours are for sputter yields of condensible (i.e., boron-containing) species only, whereas the previous work[7] accounted for all species in its differential sputter yield calculations. Non-condensible species are ignored to maintain consistency with the QCM measurements, which can only detect condensible erosion products. The corresponding values of $^{E^*}/_E$ are given in Table 7.

The contours in Fig. 5–8 indicate that as the ion incidence angle becomes more oblique, the stronger the preference towards forward sputtering becomes, as one would expect. However, Table 7 shows that the changes in $^{E^*}/_E$ differ greatly between the MD results and the QCM measurements. First, the MD results suggest that the sputtering at normal incidence is purely diffuse, whereas the QCM measurements show some non-diffuse behavior. Second, the MD results show a much stronger dependence of $^{E^*}/_E$ on the ion incidence angle than the QCM measurements over the range of 0°–45° incidence. This may mean that there is some deficiency in the sputtering model, but it is also possible that this is related to the temperature of the QCM device, as the authors of Ref. 5 noted that the QCM temperature was highly sensitive to the measurement location. Further investigation is required to determine the exact reason for the disparity

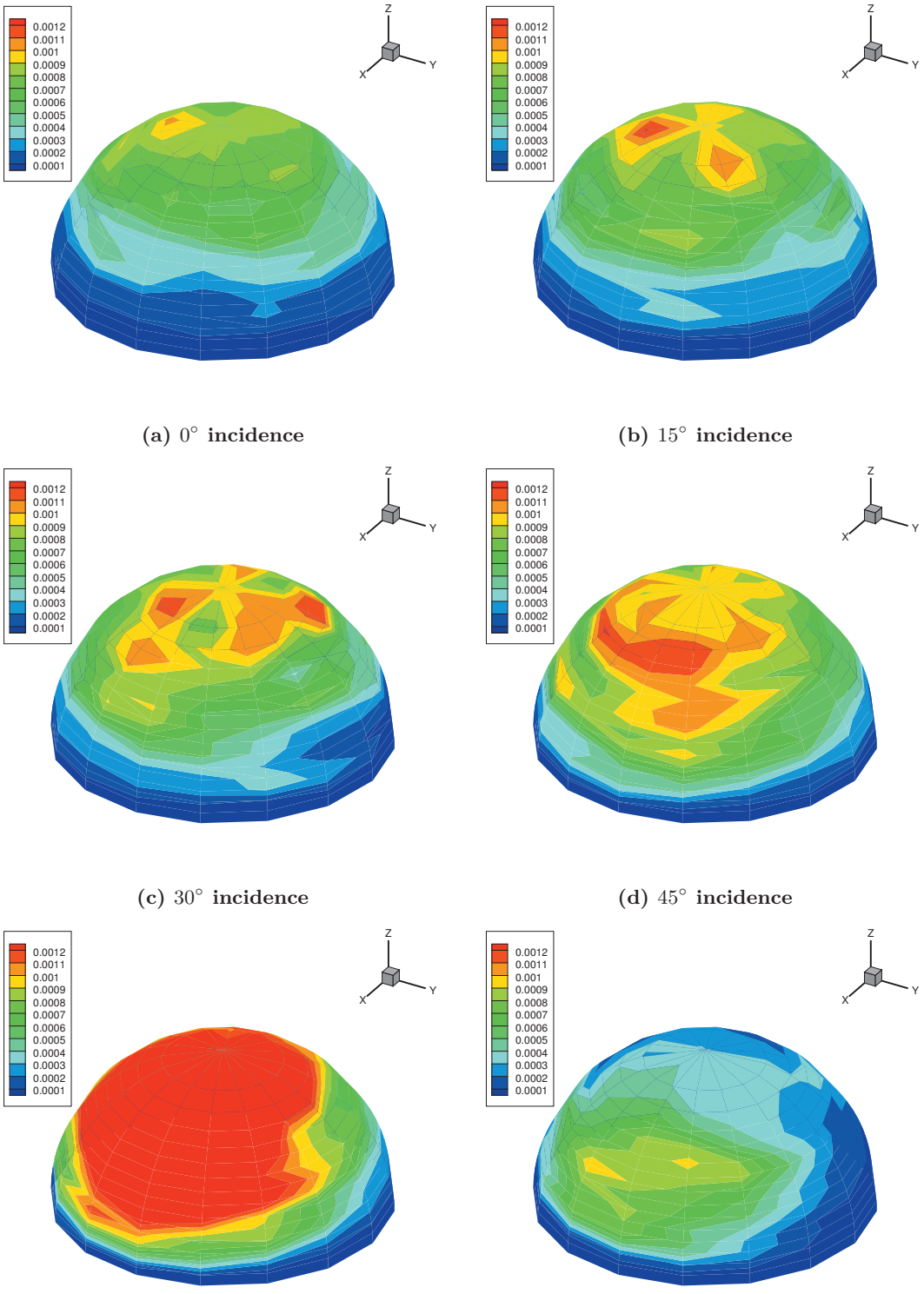

(a) 0° incidence

(b) 15° incidence

(c) 30° incidence

(d) 45° incidence

(e) 60° incidence

(f) 75° incidence

Figure 5: Calculated differential sputter yields ($mm^3/C/sr$) of condensible species at 100 eV ion energy. The positive x-axis corresponds to the forward sputtering direction.

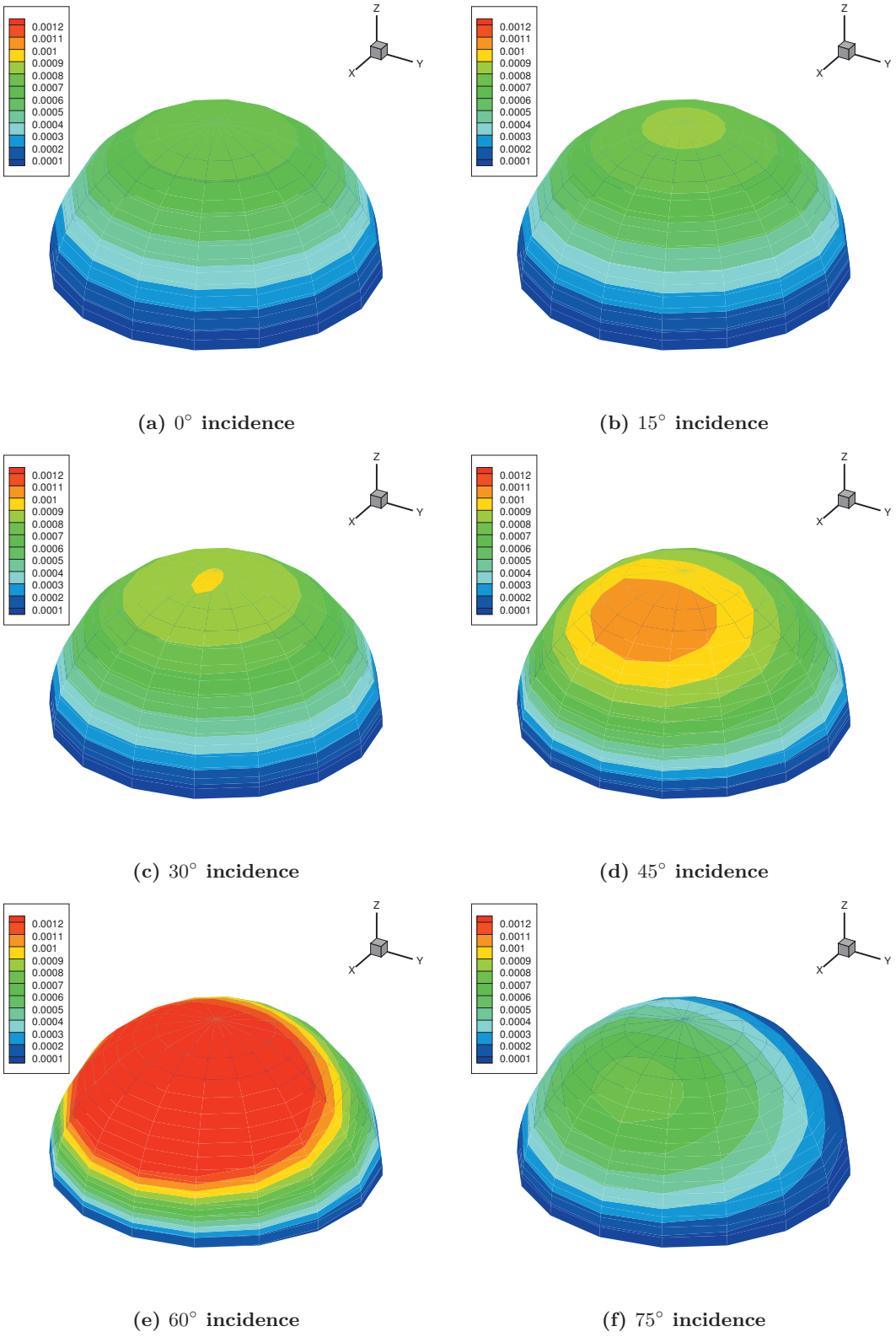

(a) 0° incidence

(b) 15° incidence

(c) 30° incidence

(d) 45° incidence

(e) 60° incidence

(f) 75° incidence

Figure 6: Modified Zhang fits to calculated differential sputter yields ($mm^3/C/sr$) of condensible species at 100 eV ion energy. The positive x-axis corresponds to the forward sputtering direction.

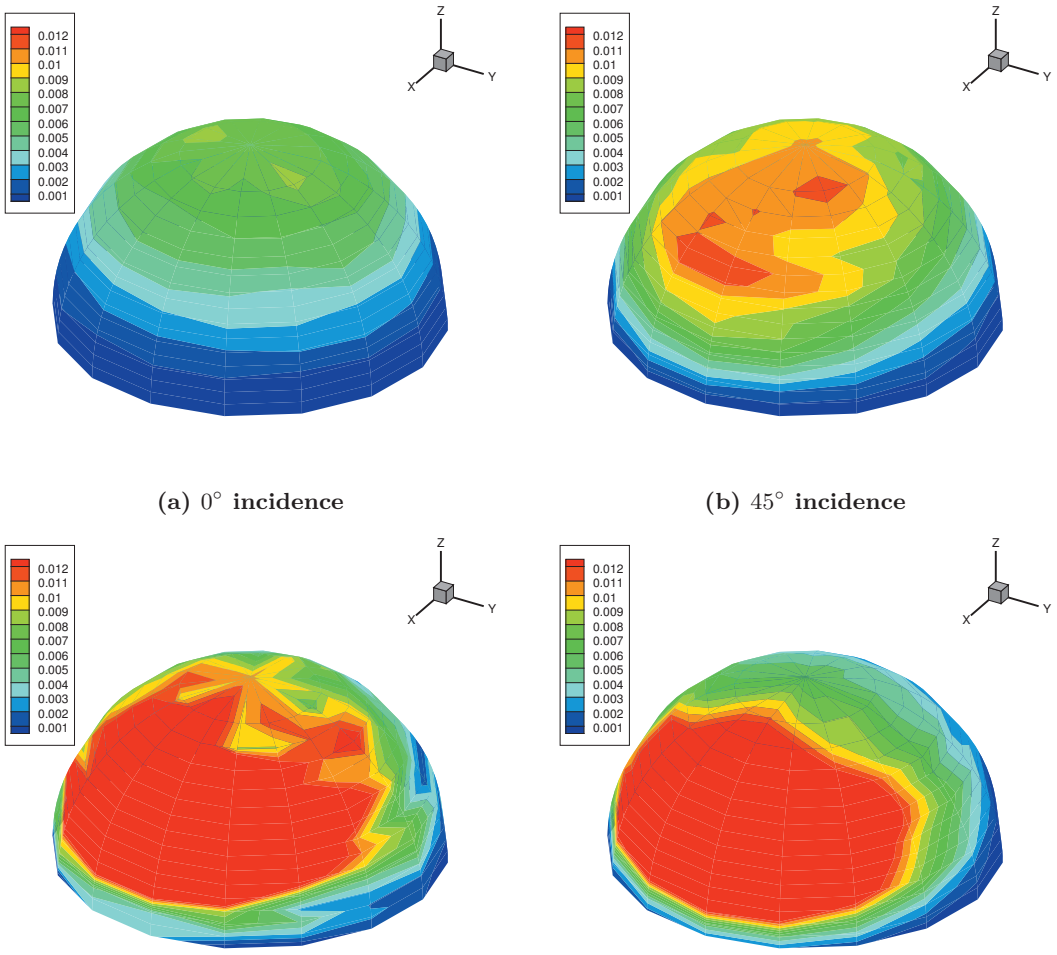

(a) 0° incidence

(b) 45° incidence

(c) 60° incidence

(d) 75° incidence

Figure 7: Calculated differential sputter yields ($mm^3/C/sr$) of condensible species at 250 eV ion energy. The positive x-axis corresponds to the forward sputtering direction.

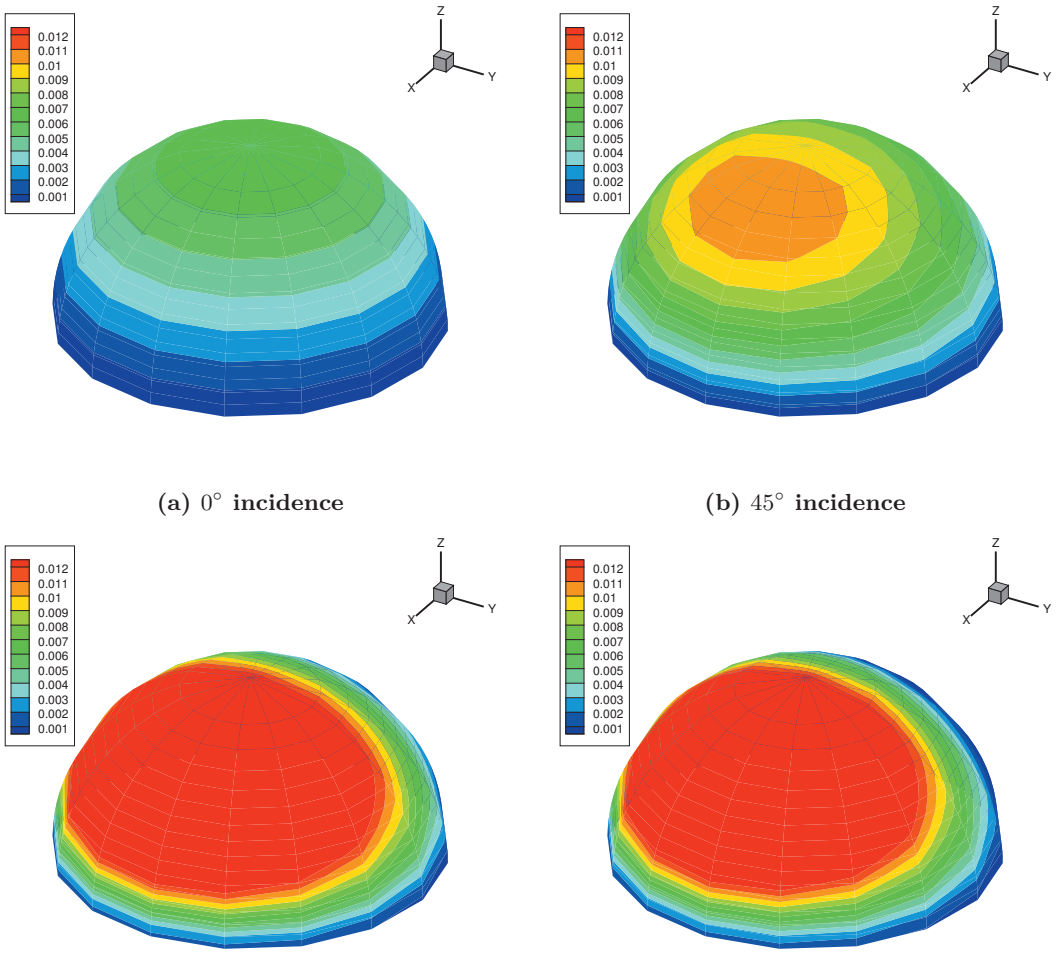

(a) 0° **incidence** **(b)** 45° **incidence**

(c) 60° **incidence** **(d)** 75° **incidence**

Figure 8: Modified Zhang fits to calculated differential sputter yields ($mm^3/C/sr$) of condensible species at 250 eV ion energy. The positive x-axis corresponds to the forward sputtering direction.

between the simulations and the experiments.

The values of $^{E^*}/_{E}$ for other simulation cases are given in Table 10 in Section III-D.

C. Atomic boron VDFs

Previous experimental[5] and computational[7] works have shown that sputtering of h-BN predominantly occurs as B_x and N_y, $x, y \geq 1$, with molecules consisting of both boron and nitrogen appearing only rarely. In particular, boron tends to be sputtered as B, whereas nitrogen tends to be sputtered as N_2. Of these, atomic boron is by far more reactive, so its transport is of greater importance in Hall thrusters.

Figure 9 shows the computed VDFs of sputtered boron atoms normal to the h-BN surface for an incident ion energy of 100 eV. Also shown are the fitted Sigmund-Thompson distributions. Table 8 shows the associated fit parameters for the Sigmund-Thompson function. The binding energy E_b is related to the effective binding velocity v_b as

$$E_b = \frac{1}{2} m_B v_b^2. \tag{14}$$

Table 8: Sigmund-Thompson VDF fit parameters for sputtering of atomic boron at 100 eV incident ion energy.

Incidence angle	E_b, eV	m_{ST}
0°	4.0	0.0
15°	4.1	0.0
30°	4.3	0.0
45°	3.9	0.0
60°	4.2	0.0
75°	4.2	0.0

The Sigmund-Thompson VDF matches the simulation results very well at all angles of incidence. Note that E_b and m_{ST}, and thus the shape of the VDF, are nearly constant with varying incidence angle at 100 eV ion energy. Note also that $m_{ST} = 0$ for all angles of incidence. These results are roughly consistent with Sigmund's linear cascade theory with the assumption of a planar energy barrier.[17] This theory suggests that the value of m_{ST} is dependent only on the energy of the incident ions, falling from about 0.2–0.3 at $E = 1$ keV to 0 as $E \to E_b$. The theory also suggests that, in the presence of a planar energy barrier at the material surface, the binding energy E_b is independent of the characteristics of the impacting ions. Although 100 eV is substantially greater than the calculated binding energy of about 4.1 eV, it otherwise appears that the MD results are consistent with the theoretical predictions. Although this conclusion may be surprising at first since h-BN is a multi-component, crystalline material, it makes sense given that the sputtering process deforms the crystal structure and depletes the surface layers of nitrogen, resulting in a layer of amorphous boron at the h-BN surface.

Tao and Yalin used laser-induced fluorescence to measure the velocity distribution of boron sputtered from an HBR-grade BN target under argon and xenon ion bombardment, and also applied Sigmund-Thompson fits to their results.[22,23] The MD results for the surface binding energy are compared with Tao's results from Ref. 22 in Table 9. Although the MD calculations appear to be less consistent than the LIF measurements, both sets of data indicate that the surface binding energy of h-BN falls between 4 eV and 6 eV. However, the values for the parameter m_{ST} differ between the numerical and experimental results. In a parametric study, Tao found that the binding energy varied from 3.9 eV to 7.2 eV as m_{ST} varied from 0 to 0.3.[23] The MD results fall within these bounds, although no parametric study has yet been performed.

Table 9: Sigmund-Thompson fit parameters as computed from the MD data and from the LIF measurements from Ref. 22. LIF measurements correspond to sputtering of HBR-grade BN under xenon ion bombardment.

Ion energy, eV	Incidence angle	E_b, eV			m_{ST}		
		MD	LIF, test 1	LIF, test 2	MD	LIF, test 1	LIF, test 2
100	0°	4.0	4.5 ± 0.6	5.0 ± 0.6	0.0	0.23 ± 0.04	0.21 ± 0.02
200	0°	5.1	4.8 ± 0.3	4.8 ± 0.4	0.0	0.24 ± 0.02	0.22 ± 0.02
300	0°	5.7	4.8 ± 0.4	4.8 ± 0.4	0.0	0.20 ± 0.03	0.23 ± 0.02
300	60°	4.2	4.3 ± 0.4	—	0.0	0.19 ± 0.04	—

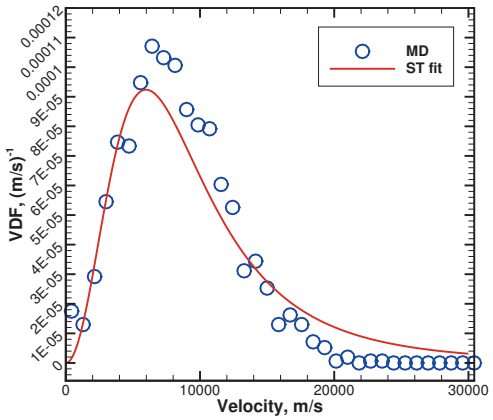

(a) 0° incidence

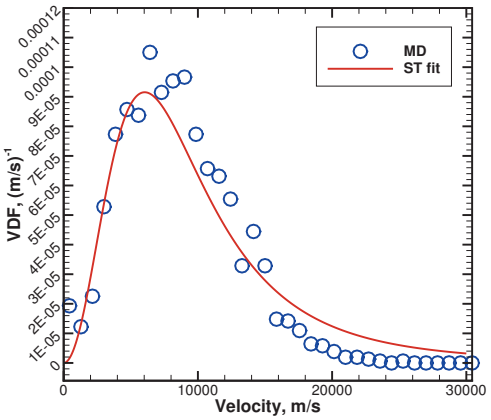

(b) 15° incidence

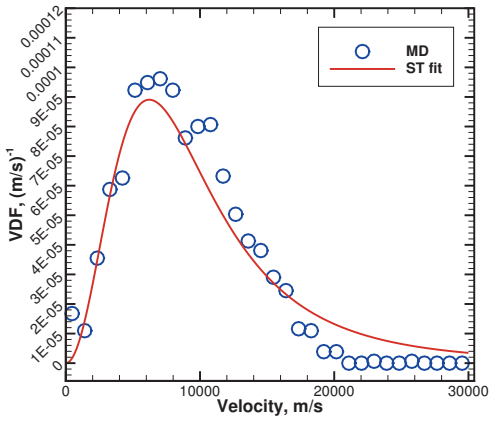

(c) 30° incidence

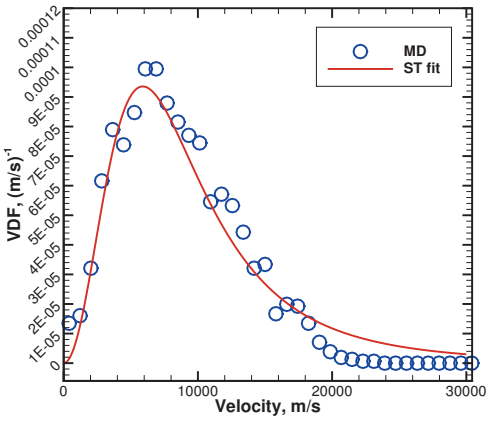

(d) 45° incidence

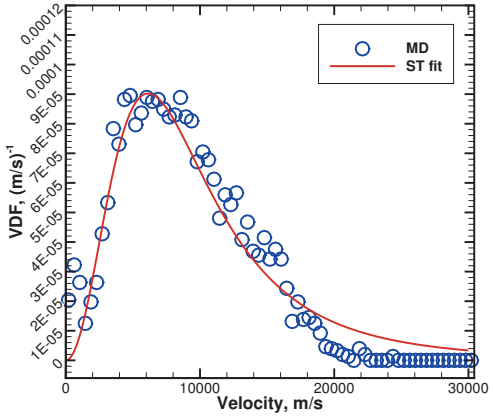

(e) 60° incidence

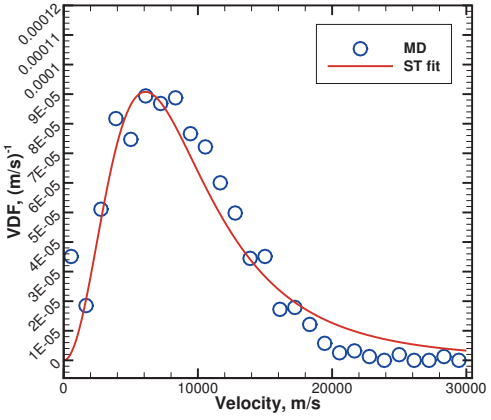

(f) 75° incidence

Figure 9: Velocity distribution functions of sputtered boron atoms normal to the *h*-BN surface. The red curves are the fitted Sigmund-Thompson distributions.

The value of the surface binding energy for the other simulation cases is reported in Table 10 in Section III-D. The mean surface binding energy from the MD results is 3.7 eV, compared to 4.8 eV from the LIF measurements for HBR-grade BN under argon and xenon ion bombardment.[22] This gives an overall error of 23% relative to the experiment. Excluding simulation cases with an ion energy less than 100 eV gives an average binding energy of 4.5 eV, or an error of 6% relative to the experiment. Even given the uncertainty with regard to m_{ST}, these results suggest that the MD model is accurately reproducing the surface binding energy observed experimentally, at least for sputtering by ions with 100 eV or greater kinetic energy. These results also imply that the apparent binding energy decreases as the incident ion energy decreases below a certain threshold. This makes sense, as a low-energy ion does not have as much energy to distribute to the atoms at the *h*-BN surface. However, it also implies that *h*-BN sputtering in the range of ion energies below about 100 eV does not fall within the linear cascade regime in which the Sigmund-Thompson distribution is valid. Additional experimental data are required to validate the MD model in this regime.

D. Tabulated sputter yield data

Table 10 shows the integrated sputter yields and values of the fit parameters ${}^{E^*}/_{E}$, E_b, and m_{ST} for all MD simulation cases. Y_{total} is computed according to Eq. 7 and Y_{est} is computed according to Eq. 8. For some simulation cases there is a significant difference between these two values. These simulation cases have not yet been run to their steady-state conditions, but the value of Y_{est} is considered a reliable estimate of the steady-state sputter yield, as demonstrated in Section II.

IV. Conclusions and future work

In this work, a molecular dynamics (MD) model was used to investigate the sputtering of hexagonal boron nitride (*h*-BN) by xenon ions. Both integrated and differential sputter yields of boron were calculated for ion energies from 40 eV to 300 eV and incidence angles from 0° to 75°. Simulations were also performed at 20 eV and 30 eV, but no sputtering occurred under those conditions. The integrated sputter yields were found to agree well with experimental measurements obtained using a quartz crystal microbalance (QCM)[5] over the range of energies investigated at normal ion incidence. A nonzero sputter yield was calculated at an ion energy as low as 40 eV, suggesting that the threshold energy for sputtering of *h*-BN is between 30 and 40 eV. Bohdansky curve fits to the sputter yields at normal incidence support this claim, giving a threshold energy of 36 ± 3 eV or 48 ± 9 eV depending on the initial parameters used. These results are consistent with the QCM measurements, which also indicate that the threshold energy lies between 30 eV and 40 eV. For a given ion energy, the sputter yields are shown to peak at an incidence angle between 60° and 70° and are well reproduced by a Yamamura curve.

Differential sputter yield calculations show that ions at oblique incidence are more likely to cause forward sputtering, as one would expect. Modified Zhang fits to the calculated yields show that the differential yields have a cosine profile at normal incidence. Comparison to the QCM measurements shows that the simulation and experiment produce different trends in the Zhang fit parameter ${}^{E^*}/_{E}$, with the MD simulations showing a positive correlation between ${}^{E^*}/_{E}$ and the ion incidence angle and the QCM results showing no dependence.

The MD data were also used to investigate the behavior of sputtered boron atoms. The velocity distribution of the boron atoms along the surface normal direction was well matched by the Sigmund-Thompson distribution predicted by linear cascade theory. The surface binding energy was calculated to be 4.5 eV on average for sputtering by ions with 100 eV or greater kinetic energy. This compared well to the results of a study using laser-induced fluorescence (LIF), which found a binding energy of 4.8 eV.[22,23] At lower ion energies, where linear cascade theory breaks down, the surface binding energy was found to decrease, indicating less energy is transferred from the ion to the atoms in the lattice.

Although the results presented in this work are very promising, further validation is required. Establishing domain independence for ion energies of 150 eV and greater would allow meaningful comparisons to existing mass loss data, which are available only for relatively high ion energies. It would also be valuable to determine the temperature dependence of the *h*-BN sputter yields, as the equilibrium temperature of 150°C used in the MD simulations is rather low compared to the expected wall temperature in a Hall thruster. Work is currently being conducted to include the model results in a Hall thruster discharge simulation, allowing comparison to *in situ* Hall thruster erosion measurements such as cavity ring-down spectroscopy[24] and prediction of the transport of boron through a thruster discharge channel.

Table 10: Calculated sputter yield, $^{E^*}/_{E}$, and surface binding energy for all MD simulations.

Ion energy, eV	Incidence angle	Y_{total}, atoms/ion	Y_{est}, atoms/ion	$^{E^*}/_{E}$	E_b, eV	m_{ST}
40	0°	0.017	0.002	0.33	0.9	0.0
	45°	0.009	0.001	0.50	2.8	0.0
	60°	0.008	0.002	0.12	2.1	0.0
	75°	0.001	0.002	1.1	0.2	0.45
60	0°	0.023	0.011	0.07	2.7	0.0
	15°	0.027	0.009	0.02	2.6	0.0
	30°	0.034	0.014	0.18	3.1	0.0
	45°	0.023	0.019	0.09	3.3	0.0
	60°	0.016	0.019	0.35	3.2	0.0
	75°	0.002	0.004	0.88	4.4	0.0
80	0°	0.075	0.043	0.0	3.4	0.0
	45°	0.13	0.040	0.56	1.0	0.36
	60°	0.075	0.073	0.32	4.1	0.0
	75°	0.039	0.013	1.0	1.5	0.22
100	0°	0.099	0.11	0.0	4.0	0.0
	15°	0.12	0.12	0.0	4.1	0.0
	30°	0.13	0.13	0.01	4.3	0.0
	45°	0.14	0.15	0.13	3.9	0.0
	60°	0.16	0.23	0.27	4.2	0.0
	75°	0.025	0.074	0.74	4.2	0.0
150	0°	0.33	0.32	0.0	4.8	0.0
	45°	0.53	0.53	0.16	4.5	0.0
	60°	0.55	0.65	0.34	4.8	0.0
	75°	0.28	0.40	0.58	6.0	0.0
200	0°	0.61	0.58	0.0	5.1	0.0
	30°	0.66	0.63	0.0	5.9	0.0
	45°	0.89	0.97	0.17	4.8	0.0
	60°	1.2	1.4	0.44	4.2	0.07
	75°	1.0	1.1	0.97	4.0	0.11
250	0°	0.90	0.90	0.0	5.7	0.0
	45°	1.3	1.4	0.15	4.8	0.08
	60°	2.4	2.1	0.61	3.2	0.19
	75°	1.9	1.7	1.2	3.1	0.21
300	0°	1.2	1.1	0.0	5.7	0.0
	60°	2.4	2.7	0.32	4.2	0.21
	75°	2.7	2.8	0.98	3.0	0.32

Acknowledgments

B. Smith would like to thank NASA for supporting this work under a NASA Space Technology Research Fellowship, grant number NNX11AM64H.

References

[1]Abashkin, V. and Gorshkov, O., "Analysis of Ceramic Erosion Characteristic in Hall-Effect Thruster with Higher Specific Impulse," IEPC Paper 2007-133, *30th International Electric Propulsion Conference*, Florence, Italy, Sept. 2007.

[2]Garnier, Y., Viel, V., Roussel, J.-F., and Bernard, J., "Low-energy xenon ion sputtering of ceramics investigated for stationary plasma thrusters," *Journal of Vacuum Science and Technology A*, Vol. 17, No. 6, 1999, pp. 3246–3254.

[3]Kim, V., Kozlov, V., Semenov, A., and Shkarban, I., "Investigation of the Boron Nitride based Ceramics Sputtering Yield Under its Bombardment by Xe and Kr ions," IEPC Paper 2001-073, *27th International Electric Propulsion Conference*, Pasadena, California, USA, Oct. 2001.

[4]Yalin, A., Surla, V., Farnell, C., Butweiller, M., and Williams, J., "Sputtering studies of multi-component materials by weight loss and cavity ring-down spectroscopy," AIAA Paper 2006-4338, *42nd AIAA/ASME/SAE/ASEE Joint Propulsion Conference & Exhibit*, Sacramento, California, USA, July 2006.

[5]Rubin, B., Topper, J., and Yalin, A., "Total and differential sputter yields of boron nitride measured by quartz crystal microbalance," *Journal of Physics D: Applied Physics*, Vol. 42, Oct. 2009, pp. 205205.

[6]Yim, J. T., Falk, M. L., and Boyd, I. D., "Modeling low energy sputtering of hexagonal boron nitride by xenon ions," *Journal of Applied Physics*, Vol. 104, No. 12, 2008, pp. 123507.

[7]Smith, B. D. and Boyd, I. D., "Computation of Total and Differential Sputter Yields of Boron Nitride Using Molecular Dynamics," IEPC Paper 2013-156, *33rd International Electric Propulsion Conference*, Washington, DC, USA, Oct. 2013.

[8]Anderson, J. a., Lorenz, C. D., and Travesset, a., "General purpose molecular dynamics simulations fully implemented on graphics processing units," *Journal of Computational Physics*, Vol. 227, No. 10, May 2008, pp. 5342–5359.

[9]Nickolls, J., Buck, I., Garland, M., and Skadron, K., "Scalable Parallel Programming with CUDA," *Queue*, Vol. 6, No. 2, March 2008, pp. 40–53.

[10]Albe, K., Möller, W., and Heinig, K., "Computer simulation and boron nitride," *Radiation Effects and Defects in Solids*, Vol. 141, No. 1-4, June 1997, pp. 85–97.

[11]Albe, K. and Möller, W., "Modelling of boron nitride: Atomic scale simulations on thin film growth," *Computational materials science*, Vol. 10, 1998, pp. 111–115.

[12]Humphrey, W., Dalke, A., and Schulten, K., "VMD – Visual Molecular Dynamics," *Journal of Molecular Graphics*, Vol. 14, 1996, pp. 33–38.

[13]Berendsen, H. J. C., Postma, J. P. M., van Gunsteren, W. F., DiNola, A., and Haak, J. R., "Molecular dynamics with coupling to an external bath," *The Journal of Chemical Physics*, Vol. 81, No. 8, Oct. 1984, pp. 3684–3690.

[14]Sun, Q. and Boyd, I. D., "Evaluation of Macroscopic Properties in the Direct Simulation Monte Carlo Method," *Journal of Thermophysics and Heat Transfer*, Vol. 19, No. 3, July 2005, pp. 329–335.

[15]Yalin, A. P., Williams, J. D., Surla, V., and Zoerb, K. A., "Differential sputter yield profiles of molybdenum due to bombardment by low energy xenon ions at normal and oblique incidence," *Journal of Physics D: Applied Physics*, Vol. 40, No. 10, May 2007, pp. 3194–3202.

[16]Zhang, Z. and Zhang, L., "Anisotropic angular distribution of sputtered atoms," *Radiation Effects and Defects in Solids*, Vol. 159, No. 5, May 2004, pp. 301–307.

[17]Sigmund, P., *Sputtering by Particle Bombardment I*, Vol. 47 of *Topics in Applied Physics*, chap. 2, Springer-Verlag, New York, 1981.

[18]Betz, G. and Wien, K., "Energy and angular distributions of sputtered particles," *International Journal of Mass Spectrometry and Ion Processes*, Vol. 140, No. 1, 1994, pp. 1–110.

[19]Bohdansky, J., "A universal relation for the sputtering yield of monatomic solids at normal ion incidence," *Nuclear Instruments and Methods in Physics Research B*, Vol. 2, No. 1-3, 1984, pp. 587–591.

[20]Yamamura, Y. and Shindo, S., "An empirical formula for angular dependence of sputtering yields," *Radiation Effects*, Vol. 80, No. 1-2, 1984, pp. 57–72.

[21]Yim, J. T., *Computational Modeling of Hall Thruster Channel Wall Erosion*, Ph.D. thesis, University of Michigan, 2008.

[22]Tao, L. and Yalin, A., "Velocity Profiles of Boron Atoms Sputtered from Boron Nitride by Low Energy Xenon Ions," IEPC Paper 2011-067, *32nd International Electric Propulsion Conference*, Wiesbaden, Germany, Sept. 2011.

[23]Tao, L. and Yalin, A., "LIF Velocity Measurement of Sputtered Boron Atoms from Boron Nitride Target," AIAA Paper 2010-6526, *46th AIAA/ASME/SAE/ASEE Joint Propulsion Conference & Exhibit*, Nashville, Tennessee, USA, July 2010.

[24]Lee, B. C., Yalin, A. P., Gallimore, A., Huang, W., and Kamhawi, H., "Real-Time Boron Nitride Erosion Measurements of the HiVHAc Thruster via Cavity Ring-Down Spectroscopy," IEPC Paper 2013-119, *33rd International Electric Propulsion Conference*, Washington, DC, USA, Oct. 2013.